Acta Astronautica 211 (2023) 795–807

Contents lists available at ScienceDirect

Acta Astronautica

journal homepage: www.elsevier.com/locate/actaastro

Research paper

Analytical determination of eclipse entry and exit points considering a conical shadow and oblate Earth☆

Marco Nugnes[1], Camilla Colombo *,[2]

Politecnico di Milano, Via La Masa 34, 20156, Milan, Italy

ARTICLE INFO

Keywords:
Eclipse
Analytical method
Conical shadow
Oblate Earth

ABSTRACT

This paper presents a new analytical procedure to model the umbra generated during an eclipse considering an oblate ellipsoid of rotation as occulting body and a conical shadow. The method is based on purely geometrical considerations and results in the analytical definition of the entry and exit points from the conical shadow starting from the knowledge of the Sun position vector, the occulting body position vector and the orbital elements of the spacecraft orbiting the occulting body. The conical shadow also permits analytical definition of the entry and exit points of the penumbra region, which cannot be defined by using the classic cylindrical approach. Some numerical applications are proposed to test the effectiveness of the analytical formulations and to check the error in the prediction of the time spent in the shadow by the satellite. Finally, a discussion between the new conical shadow model and the classic cylindrical eclipse is carried out to see the improvements introduced by the refined geometry and the effects on space missions focusing on the cumulative error when multiple revolutions are considered.

1. Introduction

Eclipses have always represented one of the most studied celestial phenomena due to their spectacularity. The prediction of the occurrence of an eclipse is not crucial when the shadowing times are small and repeating with large periods like for the Sun eclipses. However, Sidorov et al. [1] underlines how analysis of the eclipse periods becomes relevant when satellites orbiting the Earth (or another celestial body) are considered because most of them are based on solar energy and the eclipse period is important for the sizing of the batteries that should replace the solar power during this critical phase as discussed by Grey et al. [2].

There are many works dealing with the analysis of the eclipses in the literature. The first reference can be found in Escobal [3], who defines an analytical procedure to determine the true anomalies corresponding to the entry and exit points from an eclipse in the framework of classic Keplerian elements assuming the Earth's surface as a perfect sphere, and a cylindrical shadow. These assumptions simplify the modelling from a three-dimensional problem to a planar one due to the spherical symmetry and it results in a quartic equation where the unknown is the cosine of the entry/exit true anomalies. Escobal suggests also a procedure to handle the same problem modelling the Earth's surface as an oblate ellipsoid of rotation, but this time the algorithm is numerically iterative and it gives the possibility of defining the penumbra region starting from user-made assumptions related to the amplitude of the penumbra region itself. Zhang et al. [4] derives an analytical conical eclipse model for small-eccentricity orbits starting from the closed-form solution existing for circular orbits and analyses how the error in the eclipse prediction grows as the orbit eccentricity increases.

Vallado [5] presents a numerical shadow analysis for both cylindrical and conical cases starting from the same assumptions and shadow function developed by Escobal and solving the quartic polynomial equation in the true anomaly with a Newton–Raphson numerical scheme, and so no further modelling is added to the solution of the problem. Fixler [6] introduces an analytical procedure to determine the umbra and penumbra regions assuming a conical shadow and a spherical Earth resulting in another transcendental equation to be solved numerically. However, this method is based on projection of the Sun position vector onto the satellite orbital plane which slightly modifies the real geometry of the problem. Kraft [7] solves the same

☆ This document is the results of the research project funded by the European Research Council (ERC) under the European Union's Horizon 2020 research and innovation program as part of project COMPASS (Grant agreement No 679086).

* Corresponding author.
E-mail addresses: marco.nugnes@polimi.it (M. Nugnes), camilla.colombo@polimi.it (C. Colombo).
[1] PhD, Department of Aerospace Science and Technology.
[2] Associate Professor of Orbital Mechanics, Department of Aerospace Science and Technology.

https://doi.org/10.1016/j.actaastro.2023.07.007
Received 20 January 2023; Received in revised form 1 July 2023; Accepted 5 July 2023
Available online 10 July 2023

Nomenclature

a	Semi-major axis of the cone elliptical base, km
b	Semi-minor axis of the cone elliptical base, km
c	Cone height, km
$\tilde{a}$	Orbit semi-major axis, km
$\tilde{b}$	Orbit semi-minor axis, km
$\tilde{c}$	Orbit focal distance, km
d	Distance of the plane containing the cone elliptical base from the origin, km
$\hat{\mathbf{e}}$	x-axis of the perifocal reference frame
$E_{\oplus}$	Earth eccentricity according to WGS84
i	Orbit inclination, deg
$\mathbf{m}_{up}$	Angular coefficient of the upward Sun ray
$\mathbf{m}_{down}$	Angular coefficient of the downward Sun ray
$\hat{\mathbf{n}}$	Unit Sun position vector with respect to the Earth
$\hat{\mathbf{p}}$	y-axis of the perifocal reference frame
$\tilde{\mathbf{r}}$	Position vector defined in the $\tilde{x}, \tilde{y}, \tilde{z}$ frame, km
$\tilde{\mathbf{r}}_v$	Cone vertex position vector defined in the $\tilde{x}, \tilde{y}, \tilde{z}$ frame, km
$\mathbf{r}'$	Position vector defined in the x', y', z' frame, km
$\mathbf{r}_{\oplus-\odot}$	Sun position vector with respect to the Earth, km
$\mathbf{r}_{down_{\odot}}$	Leading edge position vector of the downward sun ray in the geocentric equatorial frame, km
$\mathbf{r}_{down_{\oplus}}$	Trailing edge position vector of the downward sun ray in the geocentric equatorial frame, km
$\mathbf{r}_P$	Position vector of the entry/exit point in the perifocal frame, km
$\mathbf{r}_{up_{\odot}}$	Leading edge position vector of the upward sun ray in the geocentric equatorial frame, km
$\mathbf{r}_{up_{\oplus}}$	Trailing edge position vector of the upward sun ray in the geocentric equatorial frame, km
$\mathbf{r}_{sat}$	Satellite position vector in the geocentric equatorial frame, km
R_{eq}	Earth equatorial radius, km
$\mathbf{R}_{in\rightarrow loc}$	Rotation matrix from geocentric equatorial frame to cone reference frame
$\mathbf{R}_{in\rightarrow per}$	Rotation matrix from geocentric equatorial frame to perifocal reference frame
R_{pol}	Earth polar radius, km
$\mathbf{R}$	Rotation matrix from perifocal reference frame to cone reference frame
Δt	Time period spent in the umbra shadow, s
Δt_{entry}	Time period in the penumbra before entering the umbra shadow, s
Δt_{exit}	Time period spent in the penumbra after exiting the umbra shadow, s
x, y, z	Cone reference frame
x', y', z'	Cone reference frame after rotation transformation
$\tilde{x}, \tilde{y}, \tilde{z}$	Cone reference frame after rotation and translation transformations
β	Sun angle, deg
ν^p_{entry}	True anomaly of the penumbra entry point, deg
ν^p_{exit}	True anomaly of the penumbra exit point, deg
ν^u_{entry}	True anomaly of the umbra entry point, deg
ν^u_{exit}	True anomaly of the umbra exit point, deg
Ω	Right ascension of the ascending node, deg
ω	Pericenter anomaly, deg

problem arriving at the results given by Fixler by a different derivation. The angular displacement of the Sun direction with respect to the orbit pericenter is also used by Colombo and McInnes [8] to include eclipse in the orbit dynamics expressed in terms of orbital elements assuming a planar motion in the ecliptic plane. Ortiz Longo and Rickman [9] extended the methods developed by Fixler and Kraft to a perturbed environment taking into account the effect of J_2 orbital perturbation. Montenbruck and Gill [10] used a spherical Earth conical shadow model based on the angular separation and diameters of the Sun and the Earth. The same assumptions of conical shadow model and spherical Earth have been used by Neta and Vallado [11] to compute the entry/exit points comparing the analytical solution of the cylindrical model with the numerical solution using both Newton method and Halley method. In the same paper a numerical solution to the conical shadow model is proposed using always the same iterative techniques. Srivastava et al. [12] defines a spherical Earth conical shadow methods modelling the umbra and penumbra cone geometries and using a transformation from the Earth centred inertial (ECI) frame to a Sun-centred frame.

A more complete analysis has been carried out by Dreher [13] considering also the effect of the atmospheric refraction on the light rays, but the modelling is always based on an unperturbed environment and a spherical Earth. Li et al. [14] presents a new shadow function model that uses a perspective projection based approach to solve the geometrical problem rigorously and a linear function to describe the reduction of solar radiation flux due to atmospheric effects. Vokrouhlicky et al. [15] proposed the concept of "osculating spherical Earth" to account for the errors introduced by assuming a spherical model with respect to an oblate Earth's surface.

Adhya et al. [16] are the first ones to introduce an analytical procedure for the eclipse phenomenon modelling the Earth's surface as an oblate ellipsoid of rotation. Their methodology can be used only to state if the satellite is in light, penumbra or umbra region. However, a numerical investigation by Vokrouhlicky et al. [17] has shown that the oblateness of the Earth does not bring significant differences compared to a spherical Earth for the LEO satellites. On the contrary, Woodburn [18] showed that the cylindrical assumption that neglects totally the penumbra region has important consequences for the precise numerical integration of orbit trajectories depending on the numerical scheme and the definition of the boundaries to be used for the occulted region. This can lead to relevant misprediction in high-precision orbit propagation when solar sail spacecraft are considered because solar radiation pressure (SRP) represents a major acceleration in the orbit dynamics as discussed by Zeng et al. [19].

In this paper, an analytical high-precision procedure to determine the entry and exit points from the penumbra and umbra regions is derived modelling the Earth's surface as an oblate ellipsoid of rotation and assuming a conical shadow. The methodology can be applied for all the elliptical orbits because it is based on pure geometrical considerations. The algorithm needs as input variables the inertial position vector of the occulting body and of the Sun at a given epoch together with the orbital elements of the satellite, and results in the exact inertial coordinates of the osculating orbit entry and exit points for the penumbra and umbra regions. The main assumptions used for the derivation of the formulations are the following:

(a) The Earth is modelled as an oblate ellipsoid of rotation with semi-major axis and semi-minor axis equal respectively to the Earth equatorial and polar radii.
(b) All perturbing forces are neglected.
(c) The Sun is modelled as a perfect sphere.

(d) The refraction of the light rays caused by the Earth's atmosphere is neglected.
(e) The shadow generated by the Earth is a perfect cone, that is all the light rays connecting the Sun and the Earth intersect at the same point which is the vertex of the cone.

The last assumption is the only one introducing an approximation into the modelling of the problem. However, it can be considered a good assumption because the maximum deviation between all the intersection of the light rays with the shadow axis is relatively small with respect to the astronomical distances involved in the problem.

2. Modelling

In this section all the basic mathematical transformations that will be used for the derivation of the final equation are described. The full derivation consists in considering the generic Cartesian equation of a conical surface defined in its own reference frame that must be intersected with the Cartesian equation of the elliptical orbit defined in the perifocal reference frame. This operation requires the two geometrical figures to be defined in the same reference frame so that a rotation and a translation are required.

2.1. Rotation and translation

The first mathematical transformation that is used for the derivation of the model is the rotation and translation of the Cartesian equation of the cone from its reference frame x, y, z to another generic reference system $\tilde{x}, \tilde{y}, \tilde{z}$. The generic Cartesian equation of a cone in a generic reference frame x, y, z is defined as

$$\frac{x^2}{a^2} + \frac{y^2}{b^2} - \frac{z^2}{c^2} = 0 \tag{1}$$

where a, b represent the semi-major and semi-minor axis of the ellipse obtained cutting the indefinite conical surface with the plane $z = c$. This equation defines a right cone having the vertex at the origin of the reference frame and the circular base obtained cutting the cone with a plane normal to the z-axis is an ellipse of semi-major axis and semi-minor axis equal to a and b, respectively. The first task is to express Eq. (1) in another reference system x', y', z' whose origin is coincident with the x, y, z reference frame and parallel to the final $\tilde{x}, \tilde{y}, \tilde{z}$ reference frame. Such transformation is a pure rotation that can be described mathematically by using the rotation matrix $\mathbf{R}$ which aligns the reference frame x', y', z' to the reference system x, y, z:

$$\begin{Bmatrix} x \\ y \\ z \end{Bmatrix} = \begin{bmatrix} R_{11} & R_{12} & R_{13} \\ R_{21} & R_{22} & R_{23} \\ R_{31} & R_{32} & R_{33} \end{bmatrix} \begin{Bmatrix} x' \\ y' \\ z' \end{Bmatrix} \tag{2}$$

An illustration of the rotation transformation is shown in Fig. 1.

Developing the matrix operations in Eq. (1), the transformation equations to obtain the rotation are obtained:

$$\begin{cases} x = R_{11}x' + R_{12}y' + R_{13}z' \\ y = R_{21}x' + R_{22}y' + R_{23}z' \\ z = R_{31}x' + R_{32}y' + R_{33}z' \end{cases} \tag{3}$$

It is possible to substitute Eq. (3) in place of the variables x, y, z in Eq. (1) to obtain the conical surface in terms of the x', y', z' reference frame. After some mathematical manipulation the following expression is derived to represent the Cartesian equation of a cone defined in a different reference frame:

$$\begin{aligned} &(b^2c^2R_{11}^2 + a^2c^2R_{21}^2 - a^2b^2R_{31}^2)x'^2 + (b^2c^2R_{12}^2 + \\ &+ a^2c^2R_{22}^2 - a^2b^2R_{32}^2)y'^2 + (b^2c^2R_{13}^2 + a^2c^2R_{23}^2 + \\ &- a^2b^2R_{33}^2)z'^2 + 2(b^2c^2R_{11}R_{12} + a^2c^2R_{21}R_{22} + \\ &- a^2b^2R_{31}R_{32})x'y' + 2(b^2c^2R_{11}R_{13} + a^2c^2R_{21}R_{23} + \\ &- a^2b^2R_{31}R_{33})x'z' + 2(b^2c^2R_{12}R_{13} + a^2c^2R_{22}R_{23} + \\ &- a^2b^2R_{32}R_{33})y'z' = 0 \end{aligned} \tag{4}$$

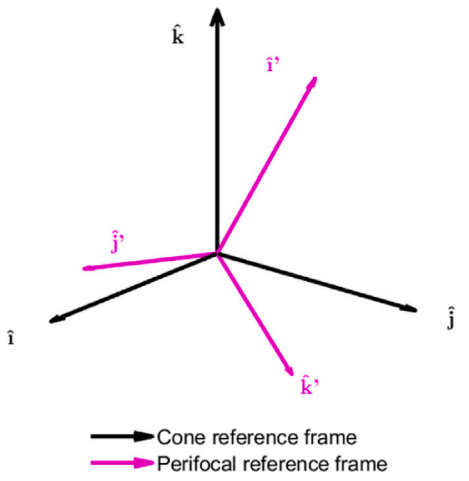

Fig. 1. General rotation problem from one reference frame to another one.

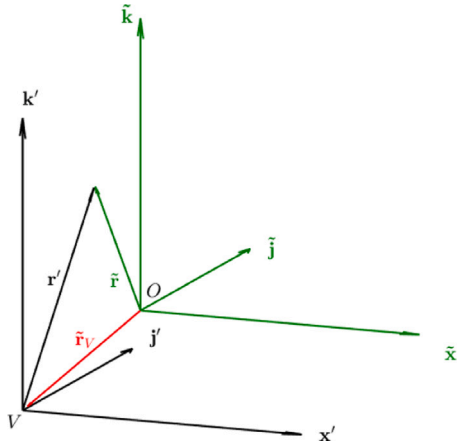

Fig. 2. General translation problem from one reference frame to another one.

Eq. (4) can be rewritten in an easier way introducing the following coefficients which are constant numbers once the rotation matrix and cone geometrical parameters are defined:

$$\begin{aligned} &\tilde{A}x'^2 + \tilde{B}y'^2 + \tilde{C}z'^2 + 2\tilde{D}x'y' + 2\tilde{E}x'z' + 2\tilde{F}y'z' = 0 \\ &\tilde{A} = b^2c^2R_{11}^2 + a^2c^2R_{21}^2 - a^2b^2R_{31}^2 \\ &\tilde{B} = b^2c^2R_{12}^2 + a^2c^2R_{22}^2 - a^2b^2R_{32}^2 \\ &\tilde{C} = b^2c^2R_{13}^2 + a^2c^2R_{23}^2 - a^2b^2R_{33}^2 \\ &\tilde{D} = b^2c^2R_{11}R_{12} + a^2c^2R_{21}R_{22} - a^2b^2R_{31}R_{32} \\ &\tilde{E} = b^2c^2R_{11}R_{13} + a^2c^2R_{21}R_{23} - a^2b^2R_{31}R_{33} \\ &\tilde{F} = b^2c^2R_{12}R_{13} + a^2c^2R_{22}R_{23} - a^2b^2R_{32}R_{33} \end{aligned} \tag{5}$$

After the rotation, Eq. (1) is expressed in the reference frame x', y', z' which is parallel to the final one $\tilde{x}, \tilde{y}, \tilde{z}$, but with a different origin. It is necessary to perform a translation transformation to align the origin of the two reference systems. In the general problem, the position vector of the vertex of the cone, $\tilde{\mathbf{r}}_\mathbf{v}$, is defined with respect to the inertial reference system. Therefore, it is better to express the translation equations considering the position vector of the origin of the x', y', z' with respect to the shifted one.

$$\tilde{\mathbf{r}} = \tilde{\mathbf{r}}_\mathbf{v} + \mathbf{r}' \tag{6}$$

A better representation of the translation transformation is shown in Fig. 2. Extending the vectorial equation and taking into account that the final aim is to express everything in the $\tilde{x}, \tilde{y}, \tilde{z}$ reference frame, the

following relations are obtained:

$$\begin{cases} x' = \tilde{x} - \tilde{x}_v \\ y' = \tilde{y} - \tilde{y}_v \\ z' = \tilde{z} - \tilde{z}_v \end{cases} \tag{7}$$

It is now possible to get the final expression of the generic conical surface defined in Eq. (1) in a new different reference frame, substituting the formulas defined in Eq. (7) inside Eq. (5):

$$\begin{aligned} &\tilde{A}\tilde{x}^2 + \tilde{B}\tilde{y}^2 + \tilde{C}\tilde{z}^2 + 2\tilde{D}\tilde{x}\tilde{y} + 2\tilde{E}\tilde{x}\tilde{z} + 2\tilde{F}\tilde{y}\tilde{z} - 2(\tilde{A}\tilde{x}_v \\ &+ \tilde{D}\tilde{y}_v + \tilde{E}\tilde{z}_v)\tilde{x} - 2(\tilde{D}\tilde{x}_v + \tilde{B}\tilde{y}_v + \tilde{F}\tilde{z}_v)\tilde{y} - 2(\tilde{E}\tilde{x}_v + \\ &+ \tilde{F}\tilde{y}_v + \tilde{C}\tilde{z}_v)\tilde{z} + (\tilde{A}\tilde{x}_v^2 + \tilde{B}\tilde{y}_v^2 + \tilde{C}\tilde{z}_v^2 + 2\tilde{D}\tilde{x}_v\tilde{y}_v + \\ &+ 2\tilde{E}\tilde{x}_v\tilde{z}_v + 2\tilde{F}\tilde{y}_v\tilde{z}_v) = 0 \end{aligned} \tag{8}$$

Again, it is possible to introduce a new variable set which are constant coefficients once the position vector of the conical surface vertex is known. This way Eq. (8) can be rewritten as

$$\begin{aligned} &\tilde{A}\tilde{x}^2 + \tilde{B}\tilde{y}^2 + \tilde{C}\tilde{z}^2 + 2\tilde{D}\tilde{x}\tilde{y} + 2\tilde{E}\tilde{x}\tilde{z} + 2\tilde{F}\tilde{y}\tilde{z} \\ &+ 2\tilde{H}\tilde{x} + 2\tilde{I}\tilde{y} + 2\tilde{J}\tilde{z} + \tilde{G} = 0 \\ &\tilde{G} = \tilde{A}\tilde{x}_v^2 + \tilde{B}\tilde{y}_v^2 + \tilde{C}\tilde{z}_v^2 + 2\tilde{D}\tilde{x}_v\tilde{y}_v + 2\tilde{E}\tilde{x}_v\tilde{z}_v \\ &+ 2\tilde{F}\tilde{y}_v\tilde{z}_v \\ &\tilde{H} = -(\tilde{A}\tilde{x}_v + \tilde{D}\tilde{y}_v + \tilde{E}\tilde{z}_v) \\ &\tilde{I} = -(\tilde{D}\tilde{x}_v + \tilde{B}\tilde{y}_v + \tilde{F}\tilde{z}_v) \\ &\tilde{J} = -(\tilde{E}\tilde{x}_v + \tilde{F}\tilde{y}_v + \tilde{C}\tilde{z}_v) \end{aligned} \tag{9}$$

The expression obtained in Eq. (9) represents the analytical expression of an elliptical conical surface characterised by a specific semi-major axis, semi-minor axis and height defined in a generic roto-translated reference system.

2.2. Intersection of the conical surface with the spacecraft orbit

The next topic to be discussed regards the intersection of the mathematical expression of the generic conical surface representing the eclipse shadow with an elliptical orbit. The intersection of the conical surfaces with the elliptical orbit requires that both the expressions are defined with respect to the same reference frame. In the previous paragraph Eq. (9) represents the Cartesian equation of a cone that can be defined in whatever reference frame once the rotation matrix and position vector of the cone vertex are defined. The expression of an elliptical orbit can be retrieved starting from the canonic equation of an ellipse.

$$\frac{\tilde{x}^2}{\tilde{a}^2} + \frac{\tilde{y}^2}{\tilde{b}^2} = 1 \tag{10}$$

where $\tilde{a}$ and $\tilde{b}$ are the semi-major axis and semi-minor axis of the ellipse, respectively. The canonic equation of the ellipse is defined with respect a reference frame centred at the centre of the ellipse. Therefore, Eq. (10) must be modified using a translation transformation because the expression of an orbit requires the Earth or the celestial body, located in one of the two foci, to be the origin of the reference frame. The analytical expression of the elliptical orbit can be obtained applying a simple translation of the origin of the reference frame knowing that the distance between the ellipse centre and the celestial body is equal to the focal distance, $\tilde{\mathbf{c}}$:

$$\tilde{\mathbf{c}} = [-\sqrt{\tilde{a}^2 - \tilde{b}^2}, 0, 0] \tag{11}$$

Looking at Fig. 3, the translation relations between the two reference systems are obtained considering:

$$\begin{cases} \bar{x} = \tilde{x} - \tilde{c} \\ \bar{y} = \tilde{y} \\ \bar{z} = \tilde{z} \end{cases} \tag{12}$$

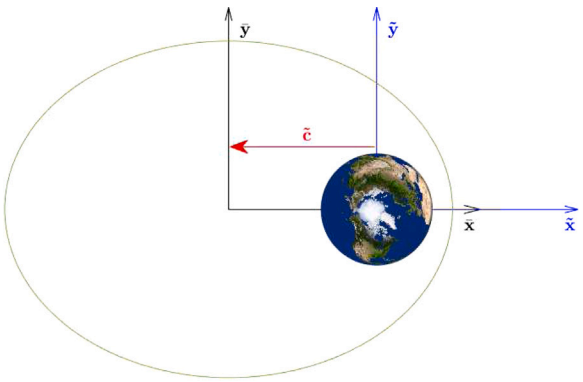

Fig. 3. Translation from ellipse centred to focal reference frame.

The analytical equation of the orbit is derived substituting Eq. (12) in Eq. (10):

$$\tilde{b}^2(\tilde{x}^2 + \tilde{c}^2 - 2\tilde{x}\tilde{c}) + \tilde{a}^2\tilde{y}^2 = \tilde{a}^2\tilde{b}^2 \tag{13}$$

The new reference frame obtained is centred in the celestial body and has the x-axis aligned with the apse line direction and the z-axis normal to the ellipse plane. Therefore, Eq. (13) represents the analytical expression of the elliptical orbit defined in the perifocal reference system usually denoted as $\hat{\mathbf{e}}$, $\hat{\mathbf{p}}$, $\hat{\mathbf{h}}$. Therefore, it is convenient to also express the conical surface in the perifocal reference frame so that the intersection between the two curves is possible. First of all, the ellipse is defined in the plane $\tilde{x}\tilde{y}$. This means that only the portion of the conical surface defined in that plane will eventually intersect the ellipse orbit. The expression of the curve associated with the conical surface in the orbital plane is obtained by imposing in Eq. (9) that $\tilde{z} = 0$.

$$\tilde{A}\tilde{x}^2 + \tilde{B}\tilde{y}^2 + 2\tilde{D}\tilde{x}\tilde{y} + 2\tilde{H}\tilde{x} + 2\tilde{I}\tilde{y} + \tilde{G} = 0 \tag{14}$$

At this point, the intersection with the elliptical orbit is carried out expressing in an explicit way the variable $\tilde{y}$ in Eq. (13):

$$\tilde{y} = \pm\frac{\tilde{b}}{\tilde{a}}\sqrt{\tilde{b}^2 - \tilde{x}^2 + 2\tilde{x}\tilde{c}} \tag{15}$$

Substituting Eq. (15) in Eq. (14) leads to the following expression.

$$\begin{aligned} &\tilde{A}\tilde{x}^2 + \tilde{B}\frac{\tilde{b}}{\tilde{a}}(\tilde{b}^2 - \tilde{x}^2 + 2\tilde{x}\tilde{c}) \pm 2\tilde{D}\tilde{x}\frac{\tilde{b}}{\tilde{a}}\sqrt{\tilde{b}^2 - \tilde{x}^2 + 2\tilde{x}\tilde{c}} \\ &+ 2\tilde{H}\tilde{x} \pm 2\tilde{I}\frac{\tilde{b}}{\tilde{a}}\sqrt{\tilde{b}^2 - \tilde{x}^2 + 2\tilde{x}\tilde{c}} + \tilde{G} = 0 \end{aligned} \tag{16}$$

It is convenient to move all the terms containing the square root at the right-hand side so that it is possible to put the square root as common factor.

$$\begin{aligned} &\bar{A}\tilde{x}^2 + \bar{B}\tilde{x} + \bar{C} = \mp 2\frac{\tilde{b}}{\tilde{a}}\sqrt{\tilde{b}^2 - \tilde{x}^2 + 2\tilde{x}\tilde{c}}\left(\tilde{D}\tilde{x} + \tilde{I}\right) \\ &\bar{A} = \left(\tilde{A} - \tilde{B}\frac{\tilde{b}^2}{\tilde{a}^2}\right) \\ &\bar{B} = 2\left(\tilde{B}\frac{\tilde{b}^2}{\tilde{a}^2}\tilde{c} + \tilde{H}\right) \\ &\bar{C} = \left(\tilde{G} + \tilde{B}\frac{\tilde{b}^2}{\tilde{a}^2}\right) \end{aligned} \tag{17}$$

To solve for the variable x which represents the unknown of the problem and corresponds to the abscissa of the entry/exit point in the perifocal reference frame, both sides of Eq. (17) are squared. In this way, the ambiguity given by the two halves of the ellipse is removed. The final equation will be a quartic equation in the unknown x. The

general solution to a quartic equation is explained in Escobal [3].

$$
\begin{aligned}
&C_1\tilde{x}^4 + C_2\tilde{x}^3 + C_3\tilde{x}^2 + C_4\tilde{x} + C_5 = 0\\
&C_1 = \bar{A}^2 + 4\tilde{D}^2\frac{\tilde{b}^2}{\tilde{a}^2}\\
&C_2 = 2\left(\bar{A}\bar{B} + 4\tilde{c}\tilde{D}^2\frac{\tilde{b}^2}{\tilde{a}^2} + 4\tilde{D}\tilde{I}\frac{\tilde{b}^2}{\tilde{a}^2}\right)\\
&C_3 = \bar{B}^2 + 2\bar{A}\bar{C} - 4\tilde{D}^2\frac{\tilde{b}^4}{\tilde{a}^2} + 4\tilde{I}^2\frac{\tilde{b}^2}{\tilde{a}^2} + 16\tilde{c}\tilde{D}\tilde{I}\frac{\tilde{b}^2}{\tilde{a}^2}\\
&C_4 = 2\bar{B}\bar{C} - 8\tilde{D}\tilde{I}\frac{\tilde{b}^4}{\tilde{a}^2} + 8\tilde{c}\tilde{I}^2\frac{\tilde{b}^2}{\tilde{a}^2}\\
&C_5 = \bar{C}^2 - 4\tilde{I}^2\frac{\tilde{b}^4}{\tilde{a}^2}
\end{aligned}
\tag{18}
$$

2.3. Solutions decision making

In the previous paragraph Eq. (18) has been derived to compute the abscissa of the entry/exit points generated by a conical shadow. This quartic equation can be solved analytically using Cardan's procedure. Three possible scenarios can occur:

i. 4 real solutions
ii. 2 real solutions and 2 complex solutions
iii. no real solutions and 4 complex solutions

In case of zero real solutions, the conical shadow is not intersecting the elliptical orbit, and so the satellite cannot be in eclipse. In case of two or four real solutions, there are four and eight possible points that are candidates for umbra and penumbra entry/exit points. Indeed, each real abscissa obtained from Eq. (18) can correspond only to a point on the upper-half or lower-half of the elliptical orbit. The ambiguity can be cancelled computing for each abscissa the point of the upper-half or lower-half of the ellipse using Eq. (15) and replacing the points in Eq. (14). If the result is not exactly zero, but a small value under a certain threshold the point belongs to the conical surface and it represents a real candidate for being an entry/exit point for the eclipse. If the condition is not satisfied the point will not lie on the conical surface and it will be discarded. This represents a first criterion that should be applied to filter for the wrong points and select the real candidates. A second ambiguity is generated because the conical surface can intersect the orbit both in the shadow and sunlight side. This time the ambiguity can be solved considering that the shadow must always be on the opposite side from the Sun. This physical condition can be exploited to write a constraint for the selection of the real entry/exit eclipse points.

$$
\mathbf{r}_{\oplus-\odot}\cdot\mathbf{r}_P < 0 \tag{19}
$$

with $\mathbf{r}_{\oplus-\odot}$ representing the position vector of the Sun with respect to the Earth considered as origin of the Geocentric Equatorial Reference frame and $\mathbf{r}_P$ the generic position vector connecting the Earth with the candidate entry/exit points on the elliptical orbit. The entry/exit points will lie in the opposite plane with respect to the Sun so that the dot product of the two vectors should be negative. The last step for the derivation of the final solution is to decide which one of the two points represents the entry and exit. The simplest way is to convert the two points into anomalies that represent the true anomalies and verifying which is the entrance and exit anomaly.

$$
\nu_P = \arccos\left(\frac{x_P}{r_P}\right) \tag{20}
$$

A picture of the ambiguities generated by the intersection of the conical surface with the elliptical orbit is presented in Fig. 4. The circular markers represent the real intersections of the conical surface with the elliptical orbit, while the triangular markers are the fake solutions coming out from the quadratic Eq. (15). The four solutions to the quartic Eq. (18) are the abscissas of the four real intersections that generate a real ordinate and a fake ordinate when the quadratic equation of the ellipse is solved.

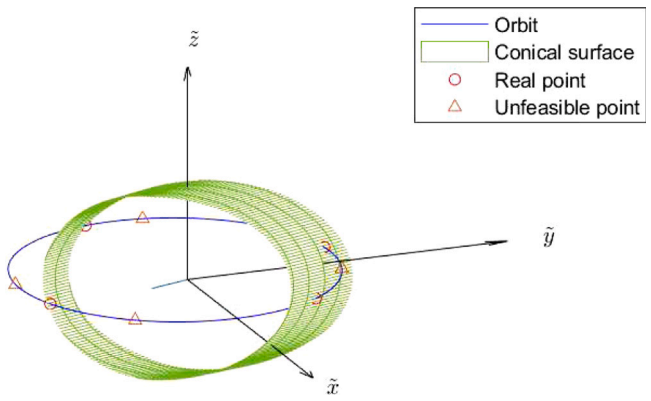

Fig. 4. Intersection of the conical surface with the elliptical orbit.

3. Orbital scenario

In the previous section, the analytical procedure devised by the authors to derive a quartic equation resulting in the intersections of a conical shadow with an elliptical orbit has been carried out. This section points out how to compute all the coefficients needed to solve for the intersection points.

3.1. Intersection eclipse with the oblate earth

The three inputs required for the algorithm are:

1. The position vector of the Sun, $\mathbf{r}_\odot$
2. Spacecraft Keplerian elements
3. The geometrical parameters of the occulting body.

The first step is to define the ellipse representing the base of the conical shadow. This cone is delimited by the Earth's surface so that the elliptical base is given by the intersection of the plane normal to the cone axis and the oblate ellipsoid associated with the Earth's surface. It is natural to assume that the axis of the conical shadow is parallel to the position vector of the Sun, $\mathbf{r}_\odot$. The Cartesian equation of the plane normal to this direction is:

$$
n_x x + n_y y + n_z z = 0 \tag{21}
$$

where n_x, n_y, n_z represent the components of the unit vector associated with $\mathbf{r}_\odot$. The second equation that is required is the one modelling the Earth's surface as an oblate ellipsoid of rotation. This equation requires the geometrical parameters of the occulting body to be known.

$$
\frac{x^2+y^2}{R_{eq}^2} + \frac{z^2}{R_{pol}^2} = 1 \tag{22}
$$

with R_{eq} and R_{pol} defining the equatorial and polar radii, respectively. The semi-major axis and semi-minor axis of the ellipse resulting from the intersection of the plane normal to the conical axis and the oblate ellipsoid can be computed as follows [20]:

$$
\begin{aligned}
a &= R_{eq}\sqrt{1 - \frac{d^2}{R_{eq}^2(1-E_\oplus^2 n_z^2)}}\\
b &= R_{pol}\frac{\sqrt{1 - d^2/R_{eq}^2 - E_\oplus^2 n_z^2}}{1 - E_\oplus^2 n_z^2}
\end{aligned}
\tag{23}
$$

where d is the distance between the plane and the origin of the reference system and it is equal to zero because this point belongs to the axis of the conical shadow, and $E_\oplus$ is the eccentricity of the occulting body. Eq. (23) provides the values of a and b to be used for the definition of the Cartesian equation of the conical surface described by Eq. (1).

3.2. Characterisation of cone vertex and rotation matrix

The last geometrical parameter that is required to define the conical surface is the cone height that is assumed to be coincident with the position vector of the cone vertex connecting the Earth centre with the cone vertex, $\mathbf{r}_v$. The following assumption is considered to determine the vertex of the cone:

Remark 1. The ellipse resulting from the intersection of the plane normal to the conical axis and passing through the Sun centre can be obtained from the ellipse representing the conical shadow basis delimited by the occulting body through an homothetic transformation.

Even if this assumption is true just in specific cases, it can be numerically proved that it is good and is not affecting the accuracy of the results provided by the algorithm. Using the previous assumption, it is possible to compute the points where the sun rays generating the conical surface depart from the intersection ellipse between the Sun's surface and the plane normal to the conical axis.

$$\begin{aligned}\mathbf{r}_{up_\odot} &= \mathbf{r}_\odot + R_\odot \hat{\mathbf{l}} \\ \mathbf{r}_{down_\odot} &= \mathbf{r}_\odot - R_\odot \hat{\mathbf{l}}\end{aligned} \tag{24}$$

where $\mathbf{r}_{up_\odot}$ and $\mathbf{r}_{down_\odot}$ are the position vectors of the leading edge of the upward and downward sun rays starting from the Sun's surface, respectively. Other two points on the Earth's surface are required to define the equations of the sun rays generating the conical shadow. These points can be defined similarly using

$$\begin{aligned}\mathbf{r}_{up_\oplus} &= R_\oplus \hat{\mathbf{l}} \\ \mathbf{r}_{down_\oplus} &= -R_\oplus \hat{\mathbf{l}}\end{aligned} \tag{25}$$

where $\mathbf{r}_{up_\oplus}$ and $\mathbf{r}_{down_\oplus}$ are the position vectors of the trailing edge of the upward and downward sun rays on the Earth's surface, respectively, and $\hat{\mathbf{l}}$ identifies the apse line direction associated with the ellipse obtained from the intersection of the oblate ellipsoid and the plane normal to conical shadow. The unit direction $\hat{\mathbf{l}}$ can be derived as

$$\hat{\mathbf{l}} = \frac{1}{\sqrt{n_x^2 + n_y^2}}[-n_y, n_x, 0] \tag{26}$$

The vertex of the cone is computed considering the intersection of the two sun rays connecting the apsidal points of the two ellipses defined on the Sun's surface and Earth's surface.

$$\begin{aligned}\mathbf{m}_{up} &= \mathbf{r}_{up_\odot} - \mathbf{r}_{up_\oplus} \\ \mathbf{m}_{down} &= \mathbf{r}_{down_\odot} - \mathbf{r}_{down_\oplus} \\ t_{int} &= \frac{x_{down_\oplus} - x_{up_\oplus}}{m_{x_{up}} - m_{x_{down}}} \\ \mathbf{r}_v &= \mathbf{r}_{up_\oplus} + t_{int}\mathbf{m}_{up}\end{aligned} \tag{27}$$

The magnitude of the vertex position vector, $\mathbf{r}_v$ is the last geometrical quantity needed to define the Cartesian equation of the conical surface, c.

$$c = \|\mathbf{r}_v\| \tag{28}$$

There is not a unique way to define the vertex of the conical shadow depending on the way the couple of points delimiting the sun rays are defined. An alternative approach to compute the position vector of the cone vertex is to consider the sun rays as the tangent lines to the ellipse obtained from the intersection of the occulting body and the conical axis passing through the points on the Sun's surface defined in Eq. (24). The equations to derive the geometrical parameters of the tangent lines are described hereafter. The first step is to intersect the general equation of a line with the analytical equation of the ellipse considered.

$$\begin{cases} y - y_p = m(x - x_p) \\ \frac{x^2}{a^2} + \frac{y^2}{b^2} = 1 \end{cases} \tag{29}$$

where x_p and y_p are the coordinates of the position vectors defined by Eq. (24) rotated in the intersection ellipse reference frame. Indeed, the canonical equation of the ellipse is valid only in a reference frame with the origin coincident with the centre of the ellipse, the x-axis aligned with the apse line direction, the y-axis aligned with the ellipse semi-minor axis and the z-axis aligned with the axis of the cone. The rotation matrix moving from the geocentric equatorial inertial frame to the ellipse local reference frame can be obtained considering the expressions of the unit vectors defined in the inertial reference frame.

$$\begin{aligned}\hat{\mathbf{e}} &= \frac{1}{\sqrt{n_x^2 + n_y^2}}[-n_y, n_x, 0] \\ \hat{\mathbf{p}} &= \frac{1}{\sqrt{n_x^2 + n_y^2}}[n_x n_z, n_y n_z, -(n_x^2 + n_y^2)] \\ \hat{\mathbf{n}} &= \frac{\mathbf{r}_\odot}{\|\mathbf{r}_\odot\|}\end{aligned} \tag{30}$$

The rotation matrix moving from the geocentric inertial reference frame to the local ellipse reference frame is obtained as

$$\mathbf{R}_{in\to loc} = \begin{bmatrix} e_x & e_y & e_z \\ p_x & p_y & p_z \\ n_x & n_y & n_z \end{bmatrix} \tag{31}$$

Substituting the general expression of a line in the canonical equation of the ellipse defines a second-order equation in the unknown x.

$$\begin{cases} y = mx + (y_p - mx_p) \\ (b^2 + a^2m^2)x^2 - 2a^2m(mx_p - y_p)x + \\ \qquad +a^2\left[(mx_p - y_p)^2 - b^2\right] = 0 \end{cases} \tag{32}$$

The second-order equation can admit only two equal solutions if the condition of tangency is applied. This means that the discriminant associated with the second-order equation is equal to 0. This condition defines a new second-order equation where the unknown is angular coefficient of the tangent lines, m.

$$a^2b^2(a^2 - x_p^2)m^2 + 2a^2b^2x_py_pm + a^2b^2(b^2 - y_p^2) = 0 \tag{33}$$

The solutions to Eq. (33) are:

$$m = \frac{-x_py_p \pm \sqrt{a^2y_p^2 + b^2x_p^2 - a^2b^2}}{a^2 - x_p^2} \tag{34}$$

At this point it is possible to substitute Eq. (34) in Eq. (33) to derive the coordinates of the tangent points.

$$x_t = \frac{a^2m(mx_p - y_p)}{b^2 + a^2m^2} \qquad y_t = mx_t + (y_p - mx_p) \tag{35}$$

The last step is to rotate from the local ellipse reference frame to the inertial reference frame the tangent points so that Eq. (27) can be applied to get the position vector of the cone vertex.

$$\mathbf{r}_{up_\oplus} = \mathbf{R}^{\mathbf{T}}{}_{in\to loc}\begin{Bmatrix} x_{up}^t \\ y_{up}^t \\ 0 \end{Bmatrix} \tag{36}$$

$$\mathbf{r}_{down_\oplus} = \mathbf{R}^{\mathbf{T}}{}_{in\to loc}\begin{Bmatrix} x_{down}^t \\ y_{down}^t \\ 0 \end{Bmatrix} \tag{37}$$

The different ways to compute the cone vertex position vertex arise from the assumptions that are modifying the real path and geometry of the sun rays because they are not creating a perfect conical surface. However, a numerical analysis where a different couple of points are used to generate the cone vertex shows that the maximum error in the definition of the magnitude of the cone vertex position vector is on the order of 1000 km corresponding to a relative error less than 1%. This small error justifies the assumption used for the derivation of

the algorithm and why the results are not considerably affected by the selection of a specific way to compute the vertex of the cone.

The last variable to be defined to get all the coefficients needed to solve the quartic equation is the rotation matrix $\mathbf{R}$ to move from the conical surface reference frame to the perifocal reference frame. This matrix can be obtained combining two different rotation matrices. Indeed, the conical surface reference frame is parallel to the local ellipse reference frame but with a different origin of the reference system. Rotation matrices are not accounting for translation so that the rotation matrix defined in Eq. (31) allows moving from the inertial frame to the local ellipse or conical surface reference frame. It is well known in orbital mechanics how to compute the rotation matrix to move from the geocentric equatorial system to the perifocal reference frame using the orbital elements of a specific orbit. The expression is reported from Battin [21]:

$$\mathbf{R}_{in\to per} = \begin{bmatrix} c\omega c\Omega - s\omega cis\Omega & -s\omega c\Omega - c\omega cis\Omega & sis\Omega \\ c\omega s\Omega + s\omega cic\Omega & -s\omega s\Omega + c\omega cic\Omega & -sic\Omega \\ s\omega si & c\omega si & ci \end{bmatrix}$$

with i, Ω, ω representing the orbit inclination, right ascension of the ascending node, and the pericenter anomaly, respectively, and the letters c and s denote the trigonometric cosine and sine functions. Combining the two rotation matrices it is possible to get the final rotation matrix which rotates the conical surface reference frame into the perifocal frame.

$$\mathbf{R} = \mathbf{R}^{\mathbf{T}}{}_{in\to per}\mathbf{R}_{in\to loc} \tag{38}$$

In this way all the geometric quantities needed to define the coefficients of Eq. (5) are known and the analytical procedure to solve the quartic equation can be applied to solve for the x-coordinate of the umbra entry/exit points defined in the perifocal reference frame.

4. Penumbra

In this section the derivation of the entry/exit penumbra points is carried out. All the analytical equations presented in Section 2 for the umbra cone are still valid also for the determination of the penumbra region. This is true because those equations are just modelling the intersection of a generic conical surface and an oblate ellipsoid of rotation.

The two methods depart in the definition of the geometrical characteristics of the conical surface and the criterion to be used for the selection of the correct solutions coming from the quartic equation. In particular, the difference in the two approaches occurs after the definition of the couple of points on the Sun's surface and occulting body surface delimiting the sun rays. The axis of the penumbra conical surface is aligned with the umbra one and also the ellipse at the base of the conical surface is the same. However, the umbra conical surface is built connecting the upper points on the Sun's surface with the upper points on the Earth's surface and the lower points on the Sun's surface with the lower points on the Earth's surface. This type of connection can be summarised in "up → up" and "down → down". A graphical representation to understand how to define the umbra and penumbra regions is presented in Fig. 5 where the upper points on the Sun's and Earth's surfaces are identified by s_{up} and E_{up}, while the downward points on the same surfaces are s_{down} and E_{down}, respectively.

The penumbra conical surface is generated by connecting the upper points on the Sun's surface to the lower points on the Earth's surface, and the lower points on the Sun's surface are connected to the upper points on the Earth's surface. This type of connection is "up → down" and "down → up". The new equations for the computation of the penumbra cone vertex are:

$$\begin{aligned} \mathbf{m}_{p_1} &= \mathbf{r}_{up_\odot} - \mathbf{r}_{down_\oplus} \\ \mathbf{m}_{p_2} &= \mathbf{r}_{down_\odot} - \mathbf{r}_{up_\oplus} \\ t^p_{int} &= \frac{x_{down_\oplus} - x_{up_\oplus}}{m_{x_{up}} - m_{x_{down}}} \\ \mathbf{r}^p_v &= \mathbf{r}_{up_\oplus} + t^p_{int}\mathbf{m}_{up} \end{aligned} \tag{39}$$

where $\mathbf{m}_{p_1}$ and $\mathbf{m}_{p_2}$ are the angular coefficients of the two penumbra lines generator, t^p_{int} is the value of the parameter to identify the penumbra vertex considering the parametric representation of a Cartesian line in 3D space, and $\mathbf{r}^p_v$ is the position vector of the penumbra cone vertex in the inertial frame.

In a similar way the second approach based on the computation of the tangent lines can be modified to get the penumbra cone vertex. For each point, Eq. (34) provides two different angular coefficients. One angular coefficient is related to the tangent line delimiting the umbra conical shadow and the second is associated with the penumbra conical surface. Therefore, after the identification of the correct angular coefficient it is possible to apply Eq. (39) to get the penumbra cone vertex.

It is obvious that the criterion used for the selection of the exact solutions coming from the quartic equations should also be modified as the penumbra conical surface is considered. The first criterion based on the selection of the points that really belong to the penumbra conical surface is unchanged. The second criterion that selects the exact points based on their positions with respect to the Sun position vector is the same if the anomalies are used but it is reversed if the distances with respect to the Sun centre are used.

5. Results

In this section the devised eclipse analytical algorithm is applied to different orbital scenarios for the determination of the entry/exit umbra and penumbra points together with the corresponding time spent in the umbra and penumbra regions. The same examples are solved also with state-of-the art eclipse algorithms based on different assumptions to verify the correctness of the results.

Four different orbital scenarios are considered:

- Low-Earth slightly inclined orbit
- Low-Earth highly inclined orbit
- Geostationary orbit
- Highly elliptical orbit

All the simulations are carried out using a processor Intel® Core (TM) i7-9750H CPU @ 2.60 GHz. The orbital parameters assumed to identify the Sun position vector are summarised in Table 1:

Table 1
Sun state vector used for all the orbital scenarios.

$r^x_\odot$	148979647.684 km
$r^y_\odot$	5289205.702 km
$r^z_\odot$	−1142.303 km
$v^x_\odot$	−0.5619 km/s
$v^y_\odot$	29.8778 km/s
$v^z_\odot$	−0.0026 km/s

5.1. Low-Earth slightly inclined orbit

The first orbital scenario deals with a satellite in a slightly inclined low-Earth orbit. The orbital parameters used for the solution of the exercise are reported in Table 2.

The entry and exit points for satellite umbra are computed using different methods. The first one is of course the new proposed analytical

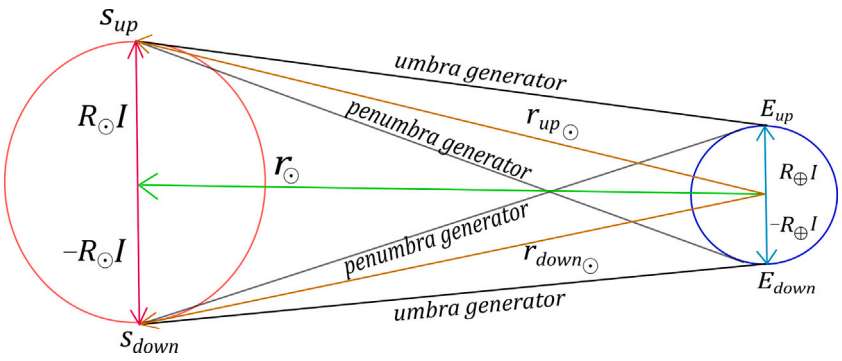

Fig. 5. Graphical representation of umbra and penumbra regions.

Table 2
Spacecraft initial orbital elements for scenario 1.

Semi-major axis	8000 km
Eccentricity	0.15
Inclination	5°
RAAN	60°
Pericenter anomaly	30°
True anomaly	140°

Table 3
Umbra entry and exit points for scenario 1.

	ν^u_{entry}	ν^u_{exit}	Δt
New approach	24.50°	138.14°	2128.53 s
Escobal cylindrical	24.19°	138.38°	2138.94 s
Fixler	24.49°	138.14°	2128.66 s
Escobal conical	24.50°	138.14°	2128.57 s

Table 4
Penumbra entry and exit points for scenario 1.

	ν^p_{entry}	ν^p_{exit}	Δt_{entry}	Δt_{exit}
New approach	23.88°	138.62°	9.16 s	11.65 s
Fixler	23.87°	138.62°	9.13 s	11.61 s
Escobal conical	23.88°	138.62°	9.17 s	11.66 s

approach. The second method is the classic Escobal cylindrical shadow model for the umbra determination. The third method is using Fixler's approach to define the same quantities. The fourth method is the iterative approach used to model the conical shadow taking into account Earth oblateness proposed by Escobal. The results computed using the different methods are presented in Table 3.

The same considerations can be done for the entry and exit penumbra points. In this case the Escobal cylindrical model cannot be considered because the assumption of cylindrical shadow does not generate a penumbra region. The results presenting the different entry and exit anomalies for the penumbra region are shown in Table 4.

5.2. Low-Earth highly inclined orbit

The second orbital scenario considers a satellite in a highly inclined low-Earth orbit. The orbital parameters used for the solution of the exercise are reported in Table 5.

The entry and exit points for satellite umbra computed using different methods are presented in Table 6.

The same considerations can be done for the entry and exit penumbra points. The results presenting the different entry and exit anomalies for the penumbra region are shown in Table 7.

Table 5
Satellite initial orbital elements for scenario 2.

Semi-major axis	8000 km
Eccentricity	0.15
Inclination	56°
RAAN	60°
Pericenter anomaly	30°
True anomaly	140°

Table 6
Umbra entry and exit points for scenario 2.

	ν^u_{entry}	ν^u_{exit}	Δt
New approach	62.73°	126.84°	1263.73 s
Escobal cylindrical	61.17°	127.52°	1305.27 s
Fixler	61.88°	126.94°	1280.13 s
Escobal conical	62.73°	126.84°	1263.84 s

Table 7
Penumbra entry and exit points for scenario 2.

	ν^p_{entry}	ν^p_{exit}	Δt_{entry}	Δt_{exit}
New approach	61.29°	128.02°	24.17 s	27.06 s
Fixler	60.46°	128.09°	23.67 s	26.72 s
Escobal conical	61.29°	128.02°	24.11 s	27.06 s

Table 8
Satellite initial orbital elements for scenario 3.

Semi-major axis	42164 km
Eccentricity	0
Inclination	0°
True anomaly	140°

Table 9
Umbra entry and exit points for scenario 3.

	ν^u_{entry}	ν^u_{exit}	Δt
New approach	83.59°	100.47°	4037.98 s
Escobal cylindrical	83.33°	100.73°	4164.81 s
Fixler	83.59°	100.47°	4038.47 s
Escobal conical	83.59°	100.47°	4037.94 s

5.3. Geosynchronous orbit

The third orbital scenario considers a satellite in a geosynchronous orbit. The orbital parameters used for the solution of the exercise are reported in Table 8.

The entry and exit points for satellite umbra computed using different methods are presented in Table 9.

The same considerations can be done for the entry and exit penumbra points. The results presenting the different entry and exit anomalies for the penumbra region are shown in Table 10.

Table 10
Penumbra entry and exit points for scenario 3.

	ν^p_{entry}	ν^p_{exit}	Δt_{entry}	Δt_{exit}
New approach	83.06°	101.0°	127.96 s	127.96 s
Fixler	83.06°	101.0°	127.51 s	127.51 s
Escobal conical	83.06°	101.0°	128.05 s	128.05 s

Table 11
Satellite initial orbital elements for scenario 4.

Semi-major axis	50000 km
Eccentricity	0.7
Inclination	10°
RAAN	20°
Pericenter anomaly	330°
True anomaly	140°

Table 12
Umbra entry and exit points for scenario 4.

	ν^u_{entry}	ν^u_{exit}	Δt
New approach	189.47°	195.44°	6696.34 s
Escobal cylindrical	189.09°	195.83°	7556.60 s
Fixler	189.14°	195.67°	6723.60 s
Escobal conical	189.47°	195.44°	6697.28 s

Table 13
Penumbra entry and exit points for scenario 4.

	ν^p_{entry}	ν^p_{exit}	Δt_{entry}	Δt_{exit}
New approach	188.75°	196.19°	847.5 s	802.2 s
Fixler	188.74°	196.20°	842.3 s	797.2 s
Escobal conical	188.75°	196.19°	846.3 s	802.1 s

5.4. Highly elliptical orbit

The fourth orbital scenario considers a satellite in a highly elliptical orbit. The orbital parameters used for the solution of the exercise are reported in Table 11.

The entry and exit points for satellite umbra computed using different methods are presented in Table 12.

The same considerations can be done for the entry and exit penumbra points. The results presenting the different entry and exit anomalies for the penumbra region are shown in Table 13.

6. Discussion

In this section the results obtained in Section 5 are discussed to compare the effectiveness of the proposed analytical method with respect to the state-of-the art algorithms.

The first consideration that should be stressed looking at all the results is that the Escobal cylindrical shadow method represents the lowest-accuracy approach to determine the umbra entry and exit points. This result was expected due to the underlying assumption of cylindrical shadow that is very coarse.

Therefore, the real comparison should be done with Fixler's method and the Escobal conical shadow method. It is important to underline the assumptions used by the two methods to compute the umbra and penumbra regions exit/entry points. Fixler's method assumes a conical shadow and a spherical Earth. It is based on solving a highly non-linear transcendental equation that represents a geometrical condition associated with the entry and exit points to/from the umbra and penumbra regions. The equation requires an initial guess to identify the four possible roots of the equations which are not known a priori. Escobal's conical model also is based on the numerical solution to a non-linear transcendental equation based on a specific shadow function and takes into account the Earth oblateness using an iterative procedure. In this case the first guess solution needed for the solution to the non-linear equation is known because it comes from the cylindrical model. Thanks to the iterative procedure Escobal's conical shadow model can be considered an accurate solution for each orbital scenario considered in the previous section. A summary of the characteristics of the different approaches is presented in Table 14.

Table 14
Summary of the main characteristics of the eclipse algorithms.

Method	Earth model	Type of solution	Shadow model
New Algorithm	O	A	CO
Escobal cylindrical	S	A	CY
Fixler	S	N	CO
Escobal conical oblate	O	N	CO

Legenda: O = Oblate, S = Sphere, CO = Conical, CY = Cylinder, A = Analytical, N = Numerical.

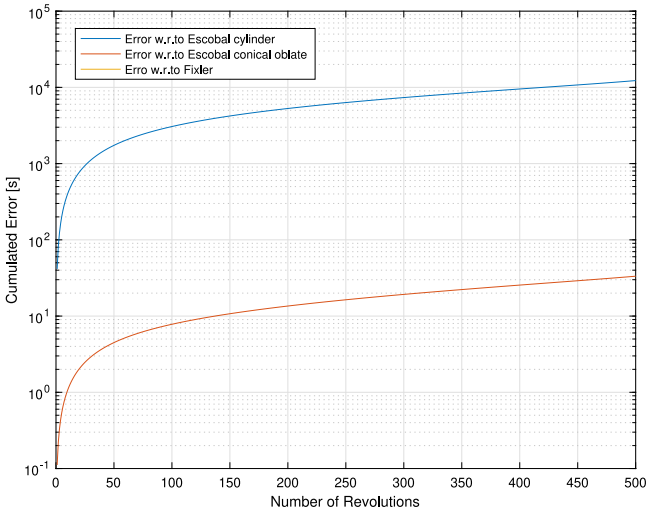

Fig. 6. Cumulative eclipse time error for scenario 2.

Looking at the different results in terms of entry and exit true anomalies and time spent in the umbra, the new proposed approach is very close to the outputs provided by Escobal's conical model. However, the proposed approach is not based on the solution of a non-linear transcendental equation and on an iterative procedure to get the correct solutions. The proposed method simply solves analytically a quartic equation and defines the correct solution of such equations providing the same accurate solution.

Even if all the different approaches are providing similar solutions it should be stressed that an error of 1-2° has a different impact according to the orbital scenario. For a low-Earth orbit where the satellite moves quite fast such error can be considered negligible, but for a highly elliptical orbit the same error in terms of anomalies can result in a significant increase in the shadow time because satellites are moving slower. It is interesting to check what happens to the eclipse time error for many satellite revolutions. A simple test has been carried out propagating the trajectory of a satellite orbiting on the highly-inclined LEO and GEO orbit proposed in scenarios 2 and 4 for a number of revolutions equal to to 500 and 300, respectively. The propagation includes the effect of J_2 orbital perturbation to improve the accuracy of the trajectory. All the different algorithms are used to compute the time spent in the umbra shadow for each revolution and the relative error with respect to the new algorithm is stored. The logarithm of the cumulative error at the end of propagation for the two scenarios are presented in Figs. 6–7.

It can be noted looking at the different scenarios that the error between the different approaches increases moving to highly inclined

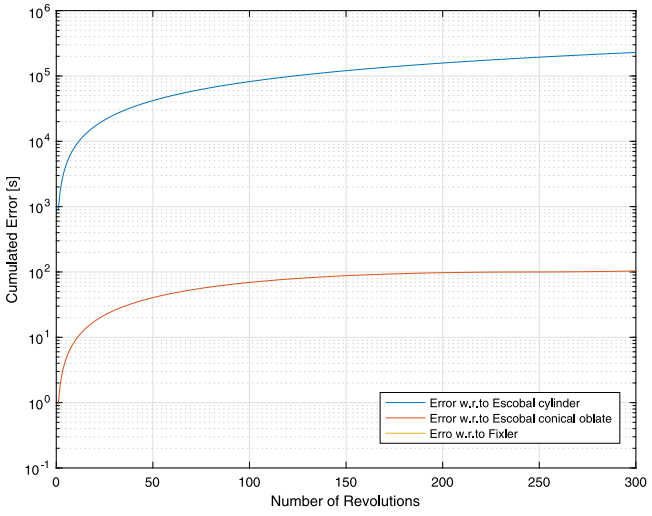

Fig. 7. Cumulative eclipse time error for scenario 4.

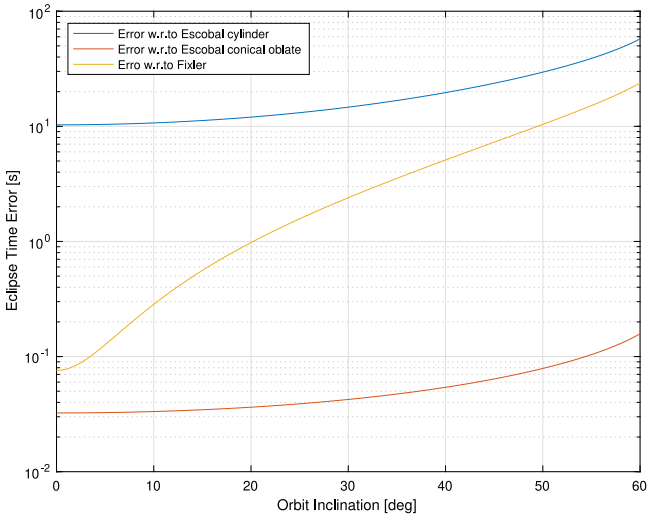

Fig. 8. Eclipse time error as function of orbit inclination for scenario 2.

orbits or highly elliptical orbits. This result was expected because in these two situations the cylindrical geometry is not a reliable way to model the actual shadow. Therefore, it is useful to perform sensitivity analysis to check how the error changes according to a change in the orbit eccentricity or inclination. This reasoning has been applied starting again from scenarios number 2 and 4. Looking at Figs. 8–9 the logarithm of the error between the time spent in the umbra shadow with respect to the one evaluated with the proposed algorithm is presented as function of the orbit inclination and eccentricity, respectively. The pictures show that the real parameter that is increasing the error in the prediction of the correct entry/exit points is the orbit inclination rather than the orbit eccentricity. This happens because Escobal's cylindrical model is based on a planar approximation of the geometry which implies that the Sun, the Earth and the satellite are always in the same plane, while Fixler's method derives its non-linear transcendental equation using the projection of the Sun position vector onto the satellite orbital plane.

The same considerations can be applied for scenario number 4. Looking at Figs. 10–11 also in this case the main parameter generating error between the different approaches is the orbit inclination. However, in this case the orbit inclination cannot increase as for the LEO case because the umbra region is definitely smaller due to the larger size of the orbit.

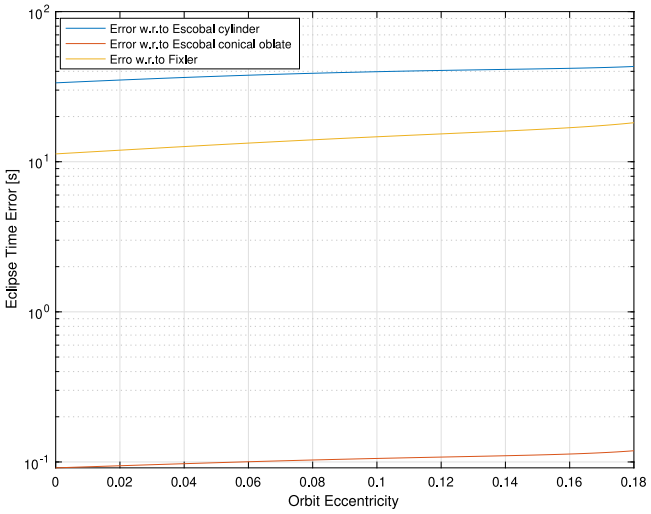

Fig. 9. Eclipse time error as function of orbit eccentricity for scenario 2.

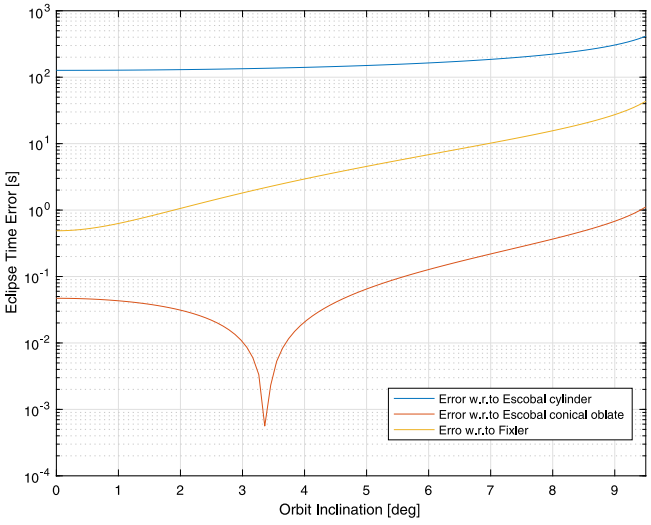

Fig. 10. Eclipse time error as function of orbit inclination for scenario 4.

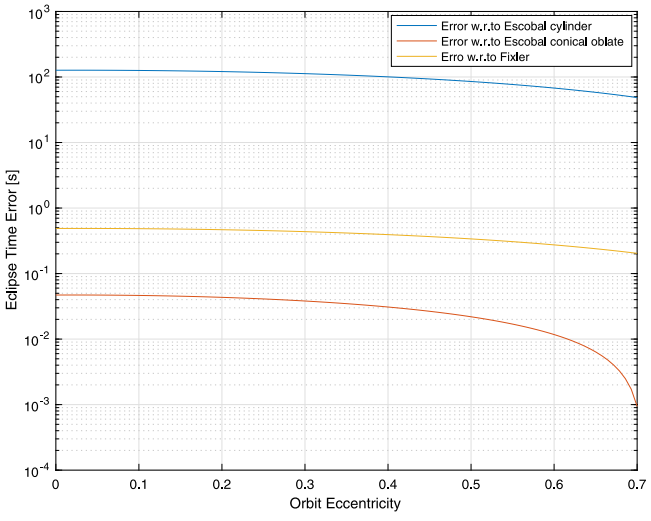

Fig. 11. Eclipse time error as function of orbit eccentricity for scenario 4.

Table 15
Average execution time over 200 simulations considering different eclipse methods.

	LEO low i	LEO high i	GEO	HEO
ECY	5.7 μs	3.0 μs	4.0 μs	5.5 μs
EC	8.3 μs	1.7 μs	4.1 μs	5.0 μs
ECO	134.4 μs	4.3 μs	148.1 μs	168.9 μs
F	95.9 μs	85.1 μs	84.4 μs	78.8 μs
A	2.7 μs	0.7 μs	2.8 μs	1.7 μs
N	15.9 μs	12.2 μs	11.6 μs	18.9 μs

Legenda: ECY = Escobal Cylindrical, EC = Escobal Conical, ECO = Escobal Conical Oblate, F = Fixler, A = Adhya, N = New Method.

The last but not least important advantage of the devised approach is related to the number and type of inputs provided. Indeed, the Sun position vector, Earth position vector and spacecraft osculating orbital elements are variables that are always known during the high-fidelity propagation because SRP and Earth oblateness perturbing accelerations must be included. Therefore, no additional variables must be computed to derive the coefficients of the quartic equation. A computational efficient analysis has been carried out to check how the analytical formulation of the proposed approach compares to the other methods. Table 15 reports the average computation time over 200 simulations for the previous orbital scenarios considering the application of the different approaches. The result of the analysis describes how the new approach is faster and more efficient compared to the conical methods counterpart. This happens because no iterative procedures must be solved and no issues associated with the initial guesses and tolerances for the iterative procedures have to be provided. Moreover, the Escobal conical oblate method defines the half-cone angle assuming the Sun and the Earth as perfect sphere specifying that this assumption is affecting the value of the angle infinitesimally [3]. The new proposed method defines the umbra and penumbra conical region considering a spherical Sun and an oblate Earth. The Adhya method [16] has been included in the analysis to show that it remains convenient with respect to the other methods if only the information regarding the state of the satellite (umbra, penumbra, sunlight) is required and it is not required to compute the entry/exit anomalies.

6.1. Error analysis according to sun angle variation

A further comparison between the proposed approach and the state-of-the art eclipse method determination can be carried out considering the impact of the Sun angle as suggested by Zhang et al. [4]. The Sun angle is the anomaly between the Sun direction and the spacecraft orbital plane. The Sun angle, usually denoted with β, is computed starting from the ecliptic longitude and obliquity following Zhang et al. [4]. Starting from an initial epoch, a simple perturbed propagator taking into account the variation of RAAN and pericenter anomaly due to J_2 has been used to include the Sun angle variation in the eclipse determination process. The analysis has been limited to the LEO highly inclined case (Table 5) which is the most relevant orbit scenario where the largest errors in terms of umbra entry/exit predictions and Sun angle variation appear. The initial epoch for the analysis is 23rd March 2022 and the propagation time is equal to 30 days. The Sun position vector, ecliptic longitude and obliquity are determined following Vallado [5]. The variation of the Sun angle as a function of propagation time is reported in Fig. 12.

The Sun angle variation permits analysis of the behaviour of the different algorithms to solve the eclipse problem considering the same spacecraft orbit. As discussed in the previous section, the analysis of the entry/exit anomaly prediction associated with the eclipse umbra considers the Escobal's cylindrical method, Escobal's conical method, Escobal's conical oblate method, Fixler's method and the proposed approach. The analysis of the penumbra limiting anomalies does not include Escobal's cylindrical method which is not able to provide a

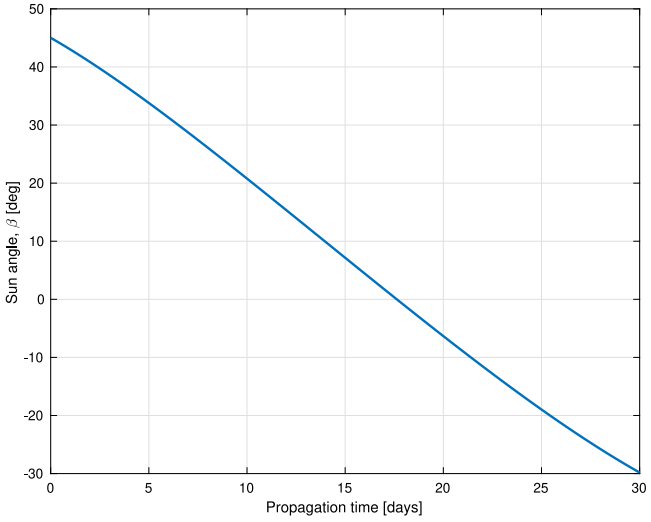

Fig. 12. Sun angle variation for LEO highly inclined case.

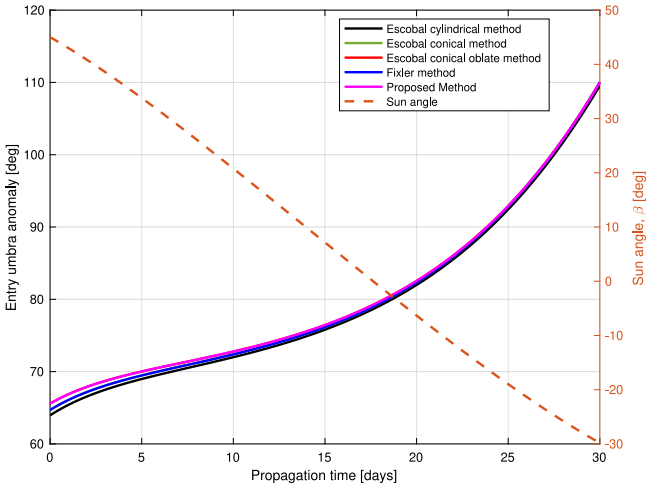

Fig. 13. Entry umbra anomaly computed with the different methods according to the sun angle variation.

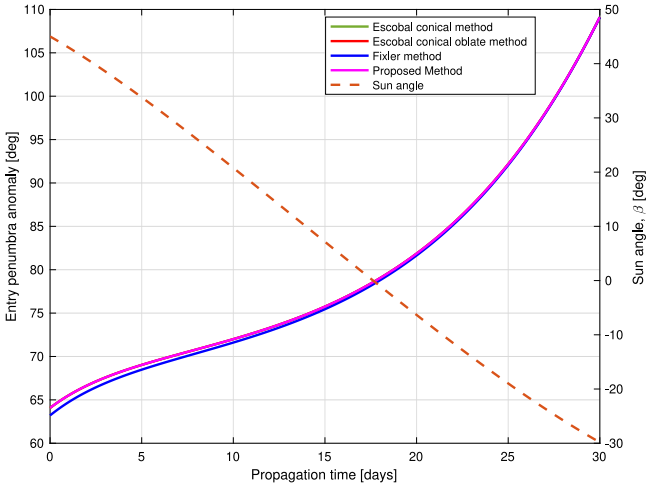

Fig. 14. Entry penumbra anomaly computed with the different methods according to the sun angle variation.

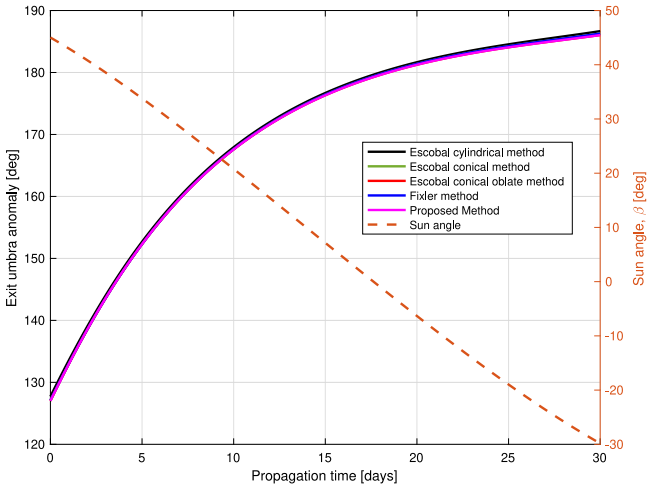

Fig. 15. Exit umbra anomaly computed with the different methods according to the sun angle variation.

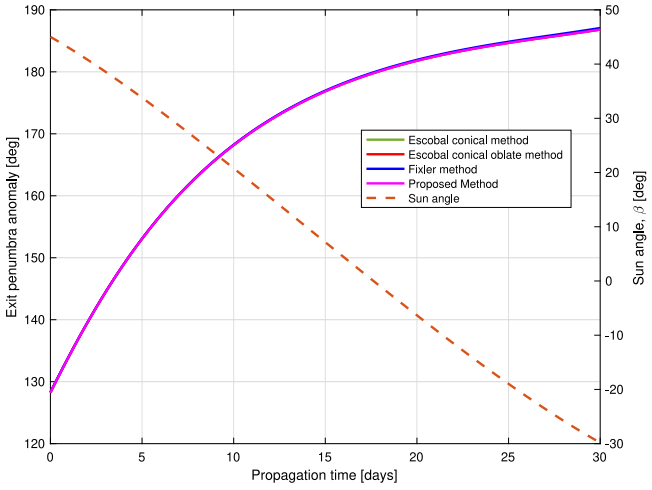

Fig. 16. Exit penumbra anomaly computed with the different methods according to the Sun angle variation.

result for the penumbra region. The results of the analysis is reported in Figs. 13–16.

To complete the analysis the logarithmic plots of the error of the proposed method and the state-of-the art ones are proposed for the different entry/exit umbra and penumbra regions to verify the accuracy of the method considering the Sun angle variation. The logarithmic plots are reported in Figs. 17–20.

7. Conclusions

In this paper a new analytical procedure for the determination of the entry and exit points of a generic satellite from the umbra and penumbra regions is presented. The method is based on the modelling of a conical surface having as axis the direction of the Sun position vector with respect to the occulting body, and an elliptical base given by the intersection of the plane normal to the cone axis and the occulting body surface modelled as an oblate ellipsoid of rotation. The conical surface is rotated and translated in the perifocal reference system so that it can be intersected with the analytical equation describing the orbit ellipse. The solutions are obtained analytically solving a quartic equation and discarding the wrong ones checking which points belong really to the conical surface and are on the opposite side with respect to the Sun.

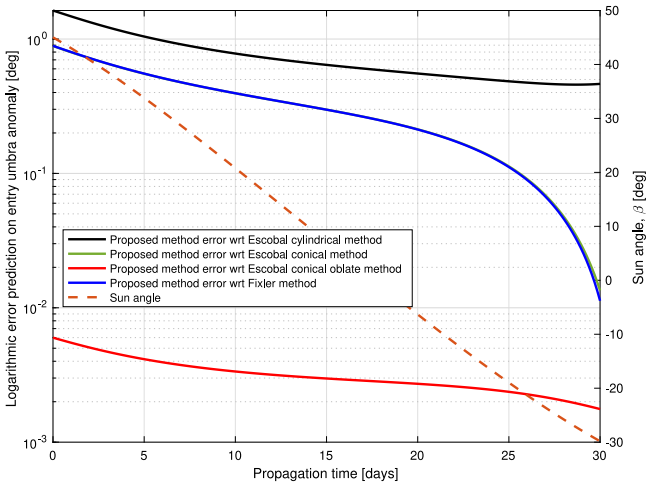

Fig. 17. Logarithmic error of entry umbra anomaly prediction with respect to the proposed method as function of the Sun angle.

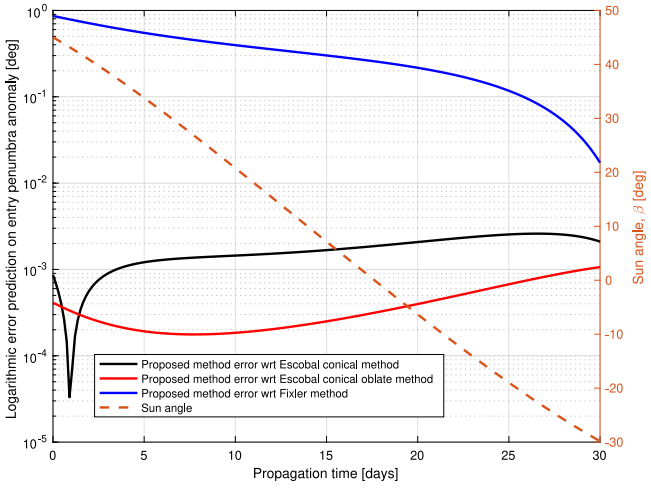

Fig. 18. Logarithmic error of entry penumbra anomaly prediction with respect to the proposed method as function of the Sun angle.

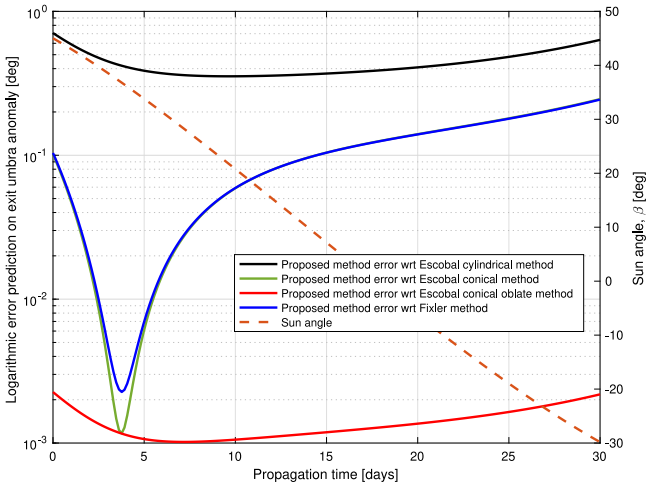

Fig. 19. Logarithmic error of exit umbra anomaly prediction with respect to the proposed method as function of the Sun angle.

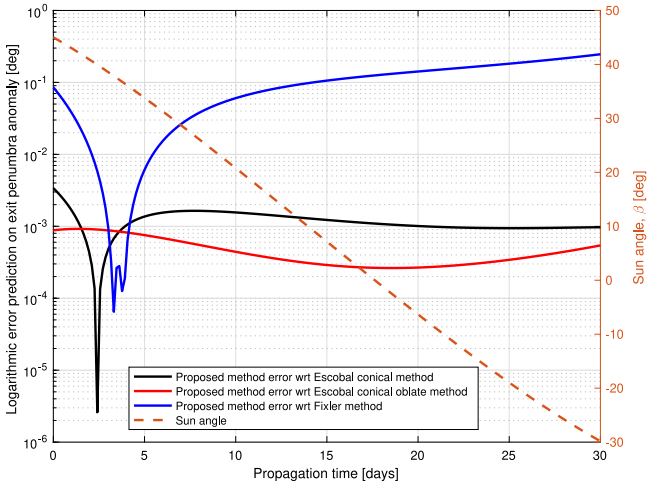

Fig. 20. Logarithmic error of exit penumbra anomaly prediction with respect to the proposed method as function of the Sun angle.

The proposed approach is applied to different relevant orbital scenarios showing that it is possible to get the same accuracy obtained using iterative and numerical methods. Further investigations are ongoing to extend the devised method also to hyperbolic orbits and to include a shadow model in the optimisation of low-thrust satellite trajectories.

Declaration of competing interest

The authors declare that they have no known competing financial interests or personal relationships that could have appeared to influence the work reported in this paper.

Acknowledgements

The research leading to these results has received funding from the European Research Council (ERC) under the European Union's Horizon 2020 research and innovation program as part of project COMPASS (Grant agreement No 679086).

References

[1] D. Sidorov, R. Dach, B. Polle, L. Prange, A. Jäggi, Adopting the empirical CODE orbit model to galileo satellites, Adv. Space Res. 66 (12) (2020) 2799–2811, http://dx.doi.org/10.1016/j.asr.2020.05.028, Scientific and Fundamental Aspects of GNSS - Part 1.

[2] J.P. Grey, I.R. Mann, M.D. Fleischauer, D.G. Elliott, Analytic model for low earth orbit satellite solar power, IEEE Trans. Aerosp. Electron. Syst. 56 (5) (2020) 3349–3359, http://dx.doi.org/10.1109/TAES.2020.3009510.

[3] P.R. Escobal, Methods of Orbit Determination, Krieger, Malabar, Florida, 1965, pp. 162–174.

[4] J. Zhang, K. Wang, B. Yan, L. Wang, Eclipse analysis for small-eccentricity orbits using analytical model, Adv. Space Res. 70 (8) (2022) 2323–2333, http://dx.doi.org/10.1016/j.asr.2022.06.071.

[5] D.A. Vallado, Fundamentals of Astrodynamics and Applications, fourth ed., in: Space Technology Library, Microcosm, Hawthorne, 2013, pp. 853–862.

[6] S.Z. Fixler, Umbra and penumbra eclipse factors for satellite orbits, AIAA J. 2 (8) (1964) 1455–1457, http://dx.doi.org/10.2514/3.2577.

[7] J.D. Kraft, A Solution for Satellite Orbit Time in Umbra and Penumbra with Application to a Lunar Satellite Mission Analysis, Technical Report N66-17237, Goddard Space Flight Center, 1965.

[8] C. Colombo, C. McInnes, Orbit design for future SpaceChip swarm missions in a planetary atmosphere, Acta Astronaut. 75 (2012) 25–41, http://dx.doi.org/10.1016/j.actaastro.2012.01.004.

[9] C.R. Ortiz Longo, S.L. Rickman, A Method for the Calculation of the Spacecraft Umbra and Penumbra Shadow Terminator Points, Technical Report 3547, Lyndon B. Johnson Space Center, 1995.

[10] O. Montenbruck, E. Gill, Satellite Orbits: Models, Methods and Applications, Springer, Berlin, 2012, pp. 802–883.

[11] B. Neta, D. Vallado, On satellite umbra/penumbra entry and exit positions, J. Astronaut. Sci. 46 (1) (1998) 91–103, http://dx.doi.org/10.1007/BF03546195.

[12] V. Srivastava, S. Yadav, Ashutosh, J. Kumar, B. Kushvah, B. Ramakrishna, P. Ekambram, Earth conical shadow modeling for LEO satellite using reference frame transformation technique: A comparative study with existing earth conical shadow models, Astron. Comput. 9 (2015) 34–39, http://dx.doi.org/10.1016/j.ascom.2014.10.001.

[13] P.E. Dreher, Satellite Shadow Time, Technical Report TMX-53389, George C. Marshall Space Flight Center, 1965.

[14] Z. Li, M. Ziebart, S. Bhattarai, D. Harrison, A shadow function model based on perspective projection and atmospheric effect for satellites in eclipse, Adv. Space Res. 63 (3) (2019) 1347–1359, http://dx.doi.org/10.1016/j.asr.2018.10.027.

[15] D. Vokrouhlicky, P. Farinella, F. Mignard, Solar radiation pressure perturbations for earth satellites: Effects of the earth polar flattening on the shadow structure and the Penumbra transitions, Astron. Astrophys. 307 (1996) 635–644.

[16] S. Adhya, A. Sibthorpe, M. Ziebart, Oblate earth eclipse state algorithm for low-earth-orbiting satellites, J. Spacecr. 41 (2003) 157–159, http://dx.doi.org/10.2514/1.1485.

[17] D. Vokrouhlicky, P. Farinella, F. Mignard, Solar radiation pressure perturbations for earth satellites: A complete theory including Penumbra transitions, Astron. Astrophys. 280 (1993) 295–312.

[18] J. Woodburn, Effects of eclipse boundary crossings on the numerical integration of orbit trajectories, in: Proceedings of the Astrodynamics Specialist Conference, Colorado, Denver, CO, 2000, pp. 116–122, http://dx.doi.org/10.2514/6.2000-4027.

[19] X. Zeng, S. Gong, J. Li, Fast solar sail rendezvous mission to near earth asteroids, Acta Astronaut. 105 (1) (2014) 40–56, http://dx.doi.org/10.1016/j.actaastro.2014.08.023.

[20] D.A. Maturi, M.Z. Ullah, S. Ahmad, F. Ahmad, An efficient computation of effective ground range using an oblate earth model, Abstr. Appl. Anal. 2014 (2014) http://dx.doi.org/10.1155/2014/459790.

[21] R.H. Battin, An Introduction to the Mathematics and Methods of Astrodynamics, AIAA Educational Series, 1999.